Analyst

PAPER

Cite this: *Analyst*, 2017, **142**, 3492

An ultrasensitive enzyme-free electrochemical immunosensor based on redox cycling amplification using methylene blue†

Gorachand Dutta [a] and Peter B. Lillehoj *[a,b]

Received 12th May 2017,
Accepted 4th August 2017

DOI: 10.1039/c7an00789b

rsc.li/analyst

We report a new enzyme-free electrochemical sensor for ultrasensitive measurements of protein biomarkers in plasma and whole blood samples based on a unique electrochemical–chemical–chemical (ECC) redox cycling signal amplification scheme. This scheme uses methylene blue (MB) as a redox indicator which undergoes an endergonic reaction with $Ru(NH_3)_6^{3+}$ and a highly exergonic reaction with tris (2-carboxyethyl)phosphine (TCEP). This approach offers improved detection sensitivity and sensor stability compared with enzyme-based ECC redox cycling techniques, while involving a simpler sensor modification process and detection protocol. This redox cycling scheme was combined with a robust immunosandwich assay for quantitative measurements of protein biomarkers. For proof of principle, *Plasmodium falciparum* histidine-rich protein 2 (*Pf*HRP2) was measured in human plasma and whole blood samples, which could be detected down to 10 fg mL^{-1} and 18 fg mL^{-1}, respectively. Furthermore, this immunosensor exhibits high selectivity, excellent reproducibility and good stability for up to 2 weeks, making it a promising platform for point-of-care testing, especially for detecting extremely low biomarker concentrations in raw biofluids.

Introduction

The ability to detect biomarkers in raw biofluids with ultrahigh sensitivity is very useful for several important biomedical applications, including early stage disease diagnosis[1,2] and diagnostic testing using non-invasive bodily fluids (*e.g.* sweat, urine, tears).[3–5] For example, ultrasensitive (<1 pg mL^{-1}) measurements of amyloid-B-derived diffusible ligands in cerebral spinal fluid can be used for early stage diagnosis of Alzheimer's disease,[6] and ultrasensitive detection of prostate specific antigen in serum can assist clinicians in monitoring disease recurrence in prostate cancer patients who have undergone radical prostatectomy.[7] Electrochemical sensors are a promising platform for biomolecular detection due to their fast response time, high sensitivity, low cost and portability.[8] Most electrochemical biosensors utilize enzymes as reporters due to their high signal generation and excellent reproducibility.[9] To achieve enhanced detection sensitivity, electrochemical sensors can be coupled with various signal amplification methods, including those based on multi-enzymatic reactions[10,11] or redox cycling.[12–15] Redox cycling is a popular technique involving repetitively-coupled reduction and oxidation reactions which increases the amount of signaling species on the sensor surface, thereby amplifying the detection signal. Signal amplification *via* redox cycling can involve multiple redox reactions, including purely chemical reactions (chemical–chemical (CC)),[16] or chemical and electrochemical reactions (electrochemical–chemical (EC), electrochemical–chemical–chemical (ECC)).[15,17–19] Of these techniques, ECC redox cycling can offer higher detection sensitivity because it involves multiple chemical/electrochemical reactions which are tailored to achieve a high signal-to-background ratio (SBR). Akanda *et al.* reported an enzymatic ECC redox cycling scheme using alkaline phosphatase (ALP) and aminophenyl phosphate (APP) as an enzyme label and substrate, respectively and a *p*-quinone imine/*p*-aminophenol (QI/AP) redox couple as an outer-sphere-reaction-philic (OSR-philic) and inner-sphere-reaction-philic (ISR-philic) couple.[20] This scheme was combined with an electrochemical sensor for ultrasensitive measurements of troponin I, which could be detected down to 10 fg mL^{-1} in serum. In a similar ECC redox cycling scheme, benzoquinone/hydroquinone (BQ/HQ) was used as an enzymatic OSR- and ISR-philic couple which could enhance the SBR by 8× compared with using a QI/AP couple.[21] While these ECC redox cycling schemes are

[a]*Department of Mechanical Engineering, Michigan State University, East Lansing, MI 48824, USA. E-mail: lillehoj@egr.msu.edu*
[b]*Department of Biomedical Engineering, Michigan State University, East Lansing, MI 48824, USA*

†Electronic supplementary information (ESI) available. See DOI: 10.1039/c7an00789b

capable of ultrasensitive measurements, they rely on enzymes which suffer from limited stability or involve complicated and time consuming testing protocols. Furthermore, existing electrochemical analytical techniques cannot achieve ultrasensitive measurements in whole blood. Thus, there is a strong need for non-enzymatic ultrasensitive electrochemical sensors that are simple to use and offer good stability.

Enzyme-free electrochemical sensors based on non-enzymatic reporters, such as metallic or graphene nanoparticles (NPs), have been reported which can offer improved shelf stability.[19,22–24] However, non-enzymatic sensors tend to suffer from diminished detection sensitivity, sluggish electrode kinetics or poor signal consistency.[25,26] To address these limitations, researchers have been developing new signal amplification strategies compatible with enzyme-free electrochemical sensors. For example, Peng *et al.* demonstrated an electrochemical immunosensor for the detection of carcinoembryonic antigen (CEA) using Fe_3O_4/Au NP labels and an AP redox cycling scheme.[19] This assay could detect CEA at concentrations down to 0.39 pg mL^{-1} in Tris buffer. Alternatively, Liu *et al.* reported an immunosensor using porous Pt NPs and PdPt nanocages for the detection of CEA and alpha-fetoprotein (AFP) using square wave voltammetry.[23] This assay exhibited lower limits of detection (LOD) of 1.4 pg mL^{-1} and 1 pg mL^{-1} for CEA and AFP, respectively, in serum samples. Singal *et al.* and Guo *et al.* also reported sensitive protein detection using graphene-modified electrodes to amplify the detection signal.[27,28] While these sensors can achieve good analytical performance, they require complicated sensor modification procedures or lack the sensitivity required for detecting very low biomarker concentrations in raw biofluids.

Here, we report a new enzyme-free immunosensor using methylene blue (MB) as a redox indicator for ultrasensitive electrochemical measurements of protein biomarkers in plasma and whole blood samples. MB is a heterocyclic organic dye which has been previously utilized for biosensing due to its excellent redox properties.[29] While enzyme-free biosensors using MB for DNA[30,31] and protein[32] detection and redox cycling[33–35] have been reported, these methods either involve complicated detection protocols or cannot achieve ultrasensitive measurements in raw biofluids. In our approach, we employ a unique ECC redox cycling scheme utilizing MB_{red}/MB_{ox} as a redox couple and $Ru(NH_3)_6^{3+}$ and TCEP as the oxidant and reductant, respectively. MB was selected for this scheme as it directly participates in the redox cycling process, circumventing the need for additional reaction species, thereby simplifying the sensor modification process and detection protocol. This scheme is coupled with a robust immunosandwich assay utilizing a MB-labelled secondary antibody for ultrasensitive measurements of *Plasmodium falciparum* histidine-rich protein 2 (*Pf*HRP2) in plasma and whole blood samples. Furthermore, this immunosensor exhibits high selectivity with minimum interference effects in human serum and whole blood, excellent reproducibility and good stability for up to 2 weeks.

Experimental

Biochemicals and reagents

Indium tin oxide (ITO) electrodes, hydrogen peroxide (H_2O_2), ammonium hydroxide (NH_4OH), (3-aminopropyl)triethoxysilane (APTES), glutaraldehyde, ethanolamine, bovine serum albumin (BSA), hexaammineruthenium(III) chloride ($Ru(NH_3)_6^{3+}$), tris(2-carboxyethyl)phosphine hydrochloride (TCEP), phosphate-buffered saline (PBS, pH 7.4) and other reagents for buffer solutions were purchased from Sigma-Aldrich (St Louis, MO). Deionized (DI) water (18.3 MΩ cm^{-1}) was generated using a Smart2Pure water purification system. A BSA–PBS solution was prepared by dissolving BSA 1% (w/v) in PBS. Mouse monoclonal anti-*Pf*HRP2 IgM (primary Ab) and mouse monoclonal anti-*Pf*HRP2 IgG (secondary Ab) were purchased from ICL, Inc. (Portland, OR). Recombinant *P. falciparum* histidine-rich protein 2 (*Pf*HRP2) and *P. falciparum* lactate dehydrogenase (*Pf*LDH) were purchased from CTK Biotech (San Diego, CA) and reconstituted using PBS. Methylene blue succinimidyl ester was purchased from Biosearch Technologies Inc. (Petaluma, CA). MB was conjugated with anti-*Pf*HRP2 IgG by coupling the amine groups of IgG and the active ester group of MB (see the ESI†) and stored at 4 °C for short-term (≤4 weeks) storage and −20 °C for long-term (several months) storage.

Sensor preparation

Electrochemical measurements were carried out using a three-electrode sensor comprising a working electrode (WE), counter electrode (CE) and reference electrode (RE). The WE consisted of ITO on glass and was prepared as previously reported[26,36,37] with minor modifications. Briefly, ITO-coated glass was cut into 1 cm × 2 cm pieces, immersed in a solution of 1 : 1 : 5 H_2O_2 (30%), NH_4OH (30%) and H_2O (v/v/v) at 70 °C for 90 min, and dried under a stream of purified N_2 gas. Hydroxylated electrodes were then immersed in 2% (v/v) APTES in anhydrous toluene for 1 h at room temperature (RT) to form a silane monolayer, followed by subsequent rinsing in anhydrous toluene, methanol, and DI water. To form an active surface for antibody immobilization, amine-functionalized electrodes were incubated in a 10% aqueous glutaraldehyde solution for 30 min at RT, rinsed in DI water, dried using N_2 gas and stored in a desiccator (30% relative humidity). Antibody immobilization was carried out by dispensing 70 μL of PBS (pH 7.4) containing 100 μg mL^{-1} of anti-*Pf*HRP2 IgM on APTES-glutaraldehyde-modified electrodes for 1 h at RT followed by thorough rinsing with DI water and drying with N_2 gas. To minimize nonspecific binding, 10 mM ethanolamine–hydrochloric acid (HCl) solution (pH 8.8) was incubated on the electrode surface for 30 min at RT, followed by rinsing twice with PBS and drying with N_2 gas. The prepared electrodes were stored at 4 °C for up to 15 days prior to measurements.

Experimental setup

Cyclic voltammetry and chronocoulometry were performed in a Teflon electrochemical cell at RT using a 620A electrochemical analyzer (CH Instruments, Austin, TX). The cell was

assembled using the prepared WE, an Ag/AgCl (3 M KCl) RE (CH Instruments), and a Pt CE (CH Instruments). TCEP/$Ru(NH_3)_6^{3+}$ solutions were prepared by combining 100 μL of PBS with 20 mM of TCEP and 100 μL of PBS containing 10 mM $Ru(NH_3)_6^{3+}$. The final concentrations of TCEP and $Ru(NH_3)_6^{3+}$ were 2 mM and 1 mM, respectively. All solutions were freshly prepared and used immediately prior to measurements.

Electrochemical measurements and data analysis

Samples were prepared by serially diluting *Pf*HRP2 or *Pf*LDH antigen in human plasma or whole blood (Bioreclamation Inc., Westbury, NY). 70 μL of spiked plasma or whole blood was dispensed onto the WE and incubated for 30 min at RT, followed by rinsing in PBS. Next, 70 μL of PBS containing 10 μg mL^{-1} of MB-labelled anti-*Pf*HRP2 IgG was dispensed onto the WE, incubated for 30 min at RT and rinsed twice with PBS. For ECC redox cycling measurements, the WE was inserted into the electrochemical cell, 1 mL of substrate was injected and incubated for 10 min followed by the application of a 0.05 V bias potential (*vs.* Ag/AgCl). Coulometric charges are taken at 100 s of chronocoulometric response profiles and each data point is plotted as the mean ± standard deviation (SD) of separate measurements obtained using new sensors. The lower LOD was calculated based on the method described in Quantitative Chemical Analysis.[38] Briefly, we determined 3× the SD of the signal at zero concentration which is represented by the dashed line in the calibration plots and the LOD was taken as the lowest detectable concentration above this +3SD line. If the concentration profile included data points below the +3SD line, the LOD was calculated as the intersection between the +3SD and linear correlation line.

Results and discussion

Electrokinetics of redox cycling using MB

A typical redox cycling scheme involves redox reactions between chemical couples occurring near (OSR-philic) and/or far (ISR-philic) from the electrode surface. The reaction rate between an ISR-philic couple and OSR-philic couple is very slow. But if a redox couple can react with both the ISR- and OSR-philic couples, it can behave as an ISR-/OSR-philic couple and enhance the electron transfer rate. In our ECC redox cycling scheme, $Ru(NH_3)_6^{3+}/Ru(NH_3)_6^{2+}$ acts as an OSR-philic couple, TCEP = O/TCEP acts as the ISR-philic couple and MB_{ox}/MB_{red} acts as an ISR-/OSR-philic couple. In the presence of TCEP, MB_{ox} is reduced to MB_{red} which subsequently reacts with $Ru(NH_3)_6^{3+}$, enhancing the electron transfer process for outer-sphere to inner-sphere redox cycling, thereby increasing the detection signal.[20] To evaluate the effectiveness of this redox cycling technique, we compared three different redox cycling schemes (Fig. 1a, c and e) using cyclic voltammetry on unmodified ITO electrodes. In the first EC redox cycling scheme (Fig. 1a), MB_{ox} is reduced by TCEP *via* a chemical reaction and MB_{red} is reoxidized *via* an electrochemical reaction with ITO. As shown in Fig. 1b, the solution containing MB_{ox} and TCEP (curve i) generated a very high anodic current due to the electro-oxidation of MB_{red}. In contrast, the cyclic voltammograms generated using solutions containing only MB_{ox} (curve ii of Fig. 1b) or TCEP (curve iii of Fig. 1b) exhibited much lower signals, indicating that EC redox cycling between MB_{ox} and TCEP effectively amplified the detection signal. Next, we investigated EC redox cycling between MB_{red} and $Ru(NH_3)_6^{3+}$ (Fig. 1c). In this scheme, $Ru(NH_3)_6^{3+}$ is reduced to $Ru(NH_3)_6^{2+}$ by MB_{red} *via* a chemical reaction and

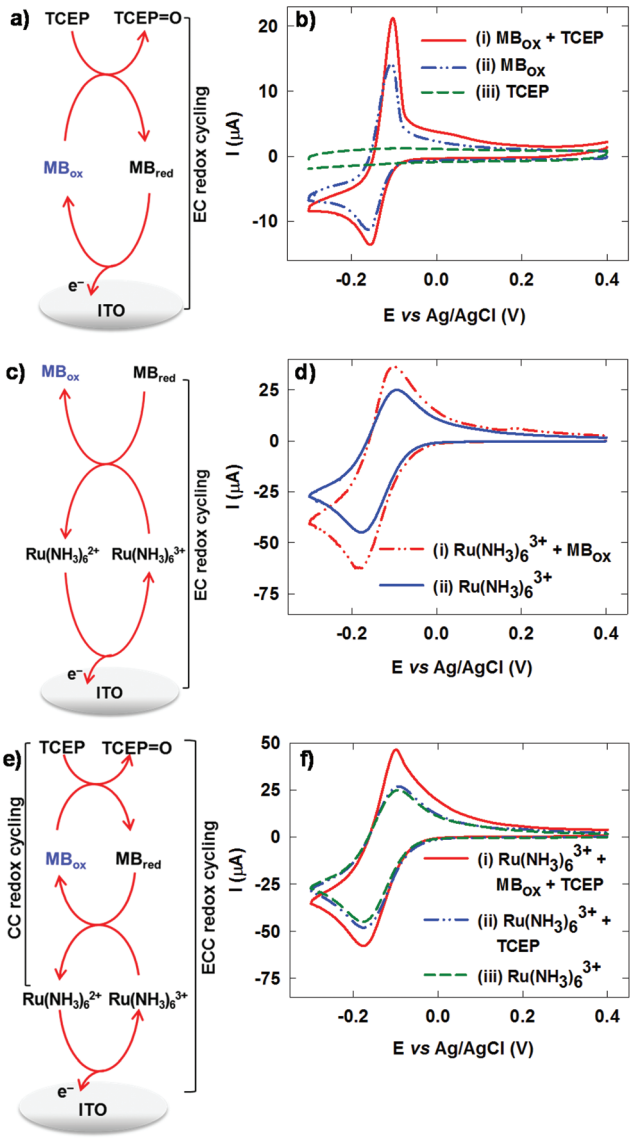

Fig. 1 (a) Schematic diagram of EC redox cycling with MB_{ox} and TCEP. (b) Cyclic voltammograms of PBS solutions containing (i) 10 μM MB_{ox} and 2 mM TCEP, (ii) 10 μM MB_{ox}, or (iii) 2 mM TCEP. (c) Schematic diagram of EC redox cycling with $Ru(NH_3)_6^{3+}$ and MB_{ox}. (d) Cyclic voltammograms of PBS solutions containing (i) 1 mM $Ru(NH_3)_6^{3+}$ and 10 μM MB_{ox}, or (ii) 1 mM $Ru(NH_3)_6^{3+}$. (e) Schematic diagram of ECC redox cycling with $Ru(NH_3)_6^{3+}$, MB_{ox}, and TCEP. (f) Cyclic voltammograms of PBS solutions containing (i) 1 mM $Ru(NH_3)_6^{3+}$, 10 μM MB_{ox} and 2 mM TCEP, (ii) 1 mM $Ru(NH_3)_6^{3+}$ and 2 mM TCEP, or (iii) 1 mM $Ru(NH_3)_6^{3+}$.

$Ru(NH_3)_6^{2+}$ is reoxidized *via* an electrochemical reaction with ITO. As shown in Fig. 1d, the solution containing $Ru(NH_3)_6^{3+}$ and MB_{ox} (curve i) generated a larger anodic current compared to the solution containing only $Ru(NH_3)_6^{3+}$ (curve ii) due to EC redox cycling. Lastly, we studied ECC redox cycling between $Ru(NH_3)_6^{3+}$, MB_{ox}, and TCEP (Fig. 1e). This scheme couples a CC reaction, where MB_{ox} is reduced to MB_{red} by TCEP and $Ru(NH_3)_6^{3+}$ is reduced to $Ru(NH_3)_6^{2+}$ by MB_{red}, with a EC reaction, and $Ru(NH_3)_6^{2+}$ undergoes electro-oxidation *via* an electrochemical reaction with ITO. These two reactions occur simultaneously resulting in substantial signal amplification. As shown in Fig. 1f, the cyclic voltammogram of the solution containing $Ru(NH_3)_6^{3+}$, MB_{ox}, and TCEP (curve i) exhibited a significantly larger anodic current compared with those generated from solutions containing $Ru(NH_3)_6^{3+}$ and TCEP (curve ii), or $Ru(NH_3)_6^{3+}$ only (curve iii). Additionally, the magnitude of the signal generated from ECC redox cycling is higher than those of the EC redox schemes (Fig. 1b and d), confirming the enhanced signal amplification achieved *via* ECC redox cycling.

In our ECC redox cycling scheme, signal amplification is achieved *via* a three-step electron transfer process. A potential diagram of the three-step electron transfer process is shown in Fig. 2a. The formal potential of each redox couple is represented by a potential well (solid line). Thermodynamically, the redox potential of MB_{ox}/MB_{red} needs to be more negative than $Ru(NH_3)_6^{3+}/Ru(NH_3)_6^{2+}$ for the chemical reduction of $Ru(NH_3)_6^{3+}$ by MB_{red}. The formal potential of the MB_{ox}/MB_{red} couple is similar to that of the $Ru(NH_3)_6^{3+}/Ru(NH_3)_6^{2+}$ couple (Fig. S1 in ESI†), enabling fast electron transfer to occur between these two couples due to a highly exergonic reaction between TCEP and MB_{ox}. Secondary side reactions (dashed lines) between $Ru(NH_3)_6^{3+}$ and TCEP, and TCEP and ITO are thermodynamically unfavorable resulting in a minimal background signal. Therefore, a high SBR can be obtained since the $Ru(NH_3)_6^{3+}/Ru(NH_3)_6^{2+}$ couple only reacts with ITO and the TCEP = O/TCEP couple does not react with ITO.[20]

To further validate these findings, chronocoulometric measurements were carried out using solutions containing different chemical species to monitor the resulting oxidation current. As shown in Fig. 2b, very low chronocoulometric signals were generated from solutions containing $Ru(NH_3)_6^{3+}$ and TCEP (curve iii), only $Ru(NH_3)_6^{3+}$ (curve iv) and only TCEP (curve v). The generation of these small coulometric charges is due to a very slow side reaction between $Ru(NH_3)_6^{3+}$ and TCEP, indicating negligible redox cycling. In contrast, a much higher (70×) chronocoulometric signal (curve ii of Fig. 2a) was generated from the solution containing MB_{ox} and TCEP due to EC redox cycling between the two species. A substantially larger (110×) signal was generated from the solution containing $Ru(NH_3)_6^{3+}$, MB_{ox} and TCEP (curve i of Fig. 2a), further validating the enhanced signal amplification generated *via* ECC redox cycling.

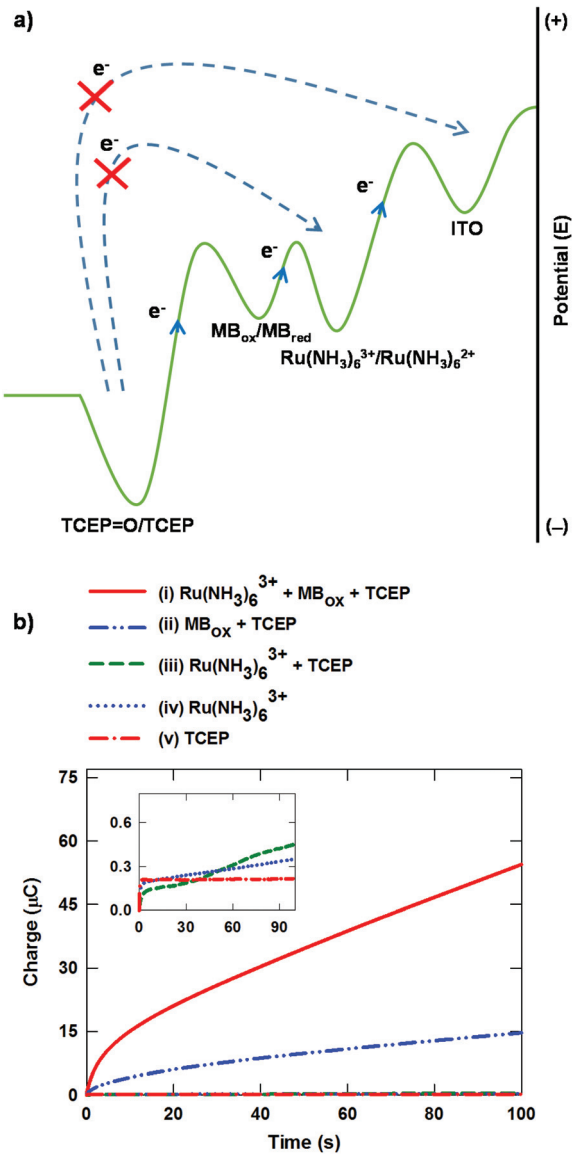

Fig. 2 (a) Potential diagram illustrating the three-step electron transfer for our ECC redox cycling scheme where formal potentials are represented by a solid line and electron transfer due to secondary side reactions are represented by dashed lines. (b) Chronocoulograms of PBS solutions containing (i) 1 mM $Ru(NH_3)_6^{3+}$, 10 μM MB_{ox} and 2 mM TCEP, (ii) 10 μM MB_{ox} and 2 mM TCEP, (iii) 1 mM $Ru(NH_3)_6^{3+}$ and 2 mM TCEP, (iv) 1 mM $Ru(NH_3)_6^{3+}$, or (v) 2 mM TCEP. Inset shows a magnified view of curves iii, iv, and v.

Optimization of assay parameters

We carried out multiple experiments to optimize several important assay parameters, such as the substrate composition, applied bias potential and incubation time. We first optimized the concentrations of $Ru(NH_3)_6^{3+}$ and TCEP since concentration variations of these species can significantly affect the rate of redox cycling.[15] Chronocoulometric measurements were carried out using solutions containing varying concentrations of $Ru(NH_3)_6^{3+}$ (Fig. S2†) and TCEP (Fig. S3†) with and without MB_{ox}. SBRs were calculated from chronocoulometric charges at 100 s of chronocoulograms. As shown in Fig. S2,† higher concentrations of $Ru(NH_3)_6^{3+}$ resulted in larger detection signals due to the generation of more $Ru(NH_3)_6^{2+}$ for subsequent oxidation with the ITO electrode.

However, when the concentration of $Ru(NH_3)_6^{3+}$ was >1 mM, the background signal became more significant due the secondary side reaction between $Ru(NH_3)_6^{3+}$ and TCEP, which lowered the SBR. A similar trend was observed with higher amounts of TECP where the background signal started becoming more significant at concentrations >2 mM (Fig. S3†). Thus, 1 mM of $Ru(NH_3)_6^{3+}$ and 2 mM of TCEP offered the optimal performance and these concentrations were selected for subsequent electrochemical measurements. We also optimized the applied bias potential using solutions containing 1 mM $Ru(NH_3)_6^{3+}$ and 2 mM TCEP with and without MB_{ox} (Fig. S4†). While increasing the bias potential, the chronocoulometric charge steadily increased and the background signals also increased correspondingly. A potential of 0.05 V was selected since it offered the optimal SBR while also minimizing any interference effects due to electroactive species in biological samples.[12,13,39] The last parameter that was optimized was the incubation time, which was tested using solutions containing $Ru(NH_3)_6^{3+}$and TCEP with and without MB_{ox} (Fig. S5†). The chronocoulometric signals increased with the increasing incubation time due to the generation of more $Ru(NH_3)_6^{2+}$ for subsequent redox cycling. However, incubating solutions for longer than 10 min caused the SBR to dramatically decrease since this can result in the secondary side reaction between $Ru(NH_3)_6^{3+}$ and TCEP to become more substantial. Therefore, a 10 min incubation time was selected.

*Pf*HRP2 detection in plasma

To assess the usefulness of our ECC redox cycling scheme for ultrasensitive analytical detection, we combined it with a robust immunosandwich assay for quantitative measurements of *Pf*HRP2. This detection scheme employs a MB-labelled antibody as a non-enzymatic reporter and ECC redox cycling using $Ru(NH_3)_6^{3+}$ and TCEP for signal amplification (Fig. 3). In the presence of *Pf*HRP2, the MB-labelled antibody becomes attached to the sensor surface *via* binding with a surface immobilized antigen. Upon application of a bias potential, a large amount of $Ru(NH_3)_6^{2+}$ is generated *via* ECC redox cycling, which amplifies the electrochemical signal. We first tested this detection scheme using human plasma spiked with *Pf*HRP2 from 10 fg mL^{-1} to 100 ng mL^{-1}. The chronocoulometric response profiles and corresponding calibration plot are shown in Fig. 4a and b, respectively. Each data point in the calibration plot is averaged over two sets of measurements performed several weeks apart with <6% variation between the two data sets, which demonstrates the high reproducibility of this assay. In addition, this assay exhibits a lower LOD of

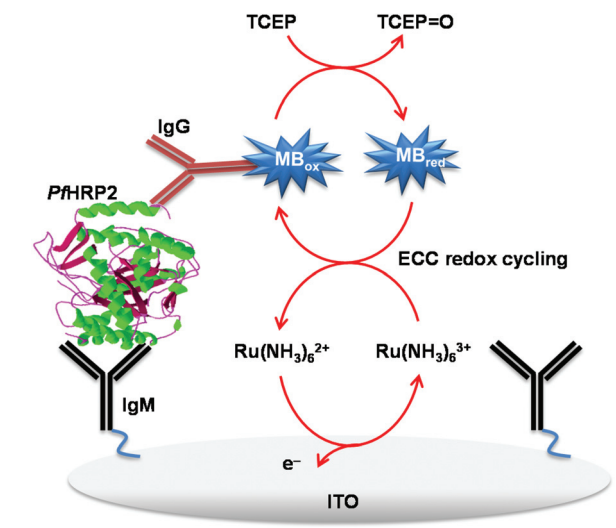

Fig. 3 Schematic of the electrochemical immunosensor incorporating ECC redox cycling using $Ru(NH_3)_6^{3+}$ and TCEP in the presence of the target antigen and MB-labeled secondary antibody.

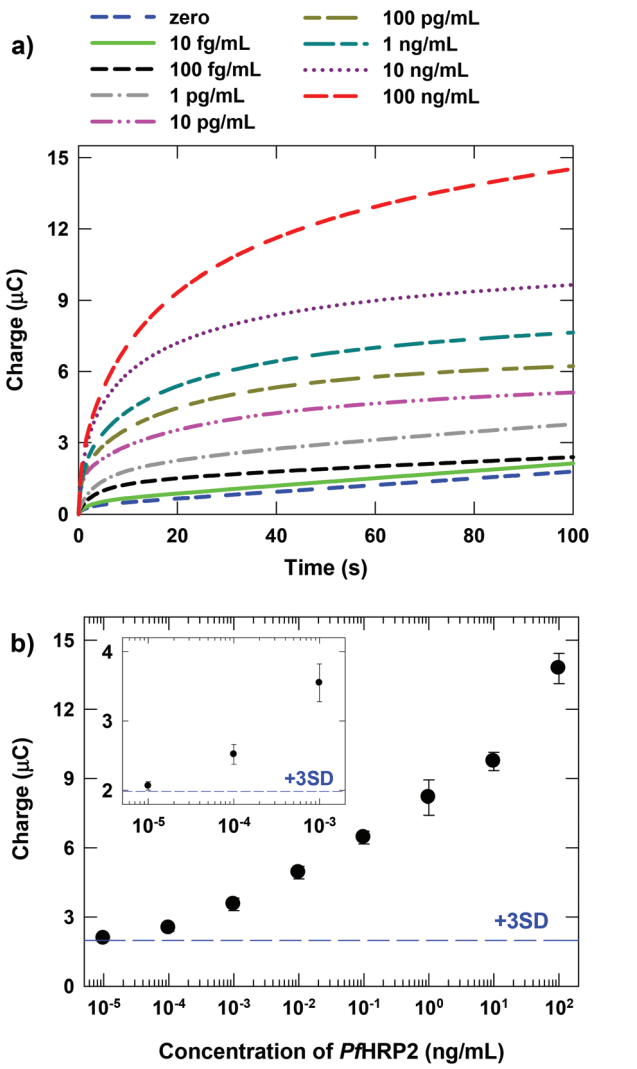

Fig. 4 (a) Chronocoulograms of human plasma spiked with *Pf*HRP2 recorded at 0.05 V (*vs.* Ag/AgCl). (b) Calibration plot based on chronocoulometric charges at 100 s from the chronocoulograms in panel a. Each data point represents the mean ± SD of six separate measurements obtained using new sensors. The dashed line corresponds to 3× the charge SD at zero concentration determined by seven measurements. Inset shows a magnified view of data points at 10 fg mL^{-1}, 100 fg mL^{-1}, and 1 pg mL^{-1}.

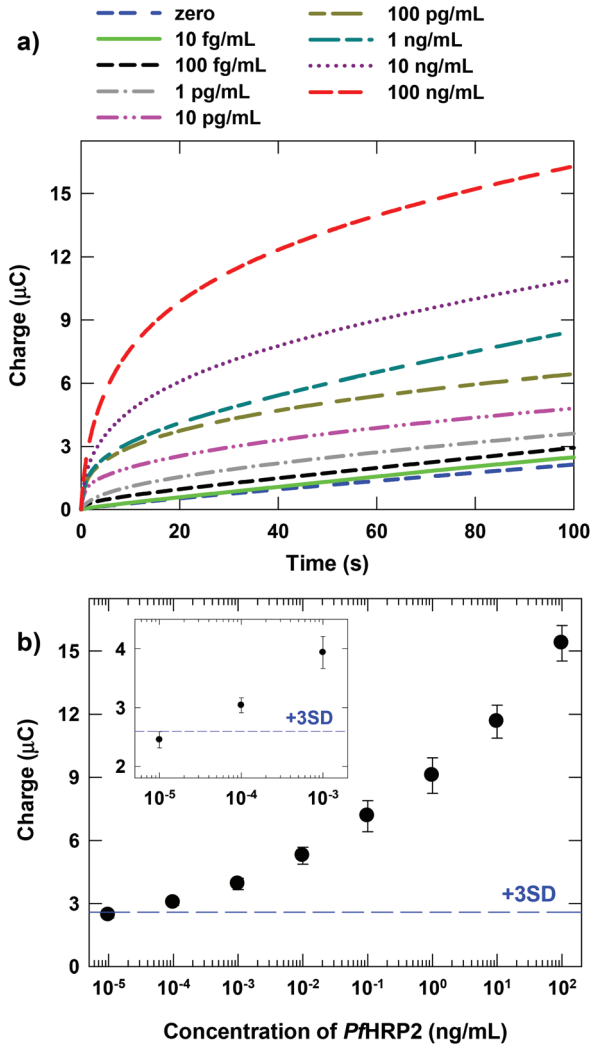

Fig. 5 (a) Chronocoulograms of whole blood spiked with *Pf*HRP2 recorded at 0.05 V (*vs.* Ag/AgCl). (b) Calibration plot based on chronocoulometric charges at 100 s from the response profile in panel a. Each data point represents the mean ± SD of six separate measurements obtained using new sensors. The dashed line corresponds to 3× the charge SD at zero concentration determined by seven measurements. Inset shows a magnified view of the data points at 10 fg mL^{-1}, 100 fg mL^{-1}, and 1 pg mL^{-1}.

10 fg mL^{-1} in plasma, which is 30× lower than previously reported enzyme-free electrochemical immunosensors.[40]

*Pf*HRP2 detection in whole blood

*Pf*HRP2 measurements were also performed using whole blood samples spiked with *Pf*HRP2 from 10 fg mL^{-1} to 100 ng mL^{-1}. The chronocoulometric response profiles and corresponding calibration plot are shown in Fig. 5a and b, respectively. The analytical performance of the whole blood assay is comparable to that of the plasma assay (Fig. 4), which also exhibits good reproducibility (<10% variation between two separate data sets obtained weeks apart) and ultrahigh sensitivity with a lower LOD of 18 fg mL^{-1}. The slightly higher LOD in blood is likely due to the presence of additional components (*e.g.* cells, platelets) compared with plasma. Nonetheless, these results demonstrate the capability of this sensor to achieve ultrasensitive measurements of protein biomarkers in whole blood samples. A comparison of our biosensor technology with previously reported enzyme-free electrochemical immunosensors is presented in Table 1 and shows that our biosensor offers superior performance with regard to a wider detection range and lower LOD in complex matrices (*i.e.* whole blood).

Assay specificity and stability

The specificity of this sensor was briefly studied by performing measurements of whole blood samples spiked with *Pf*LDH, which is another malaria biomarker found in patients with *P. falciparum* infection, and non-spiked blood samples. As shown in Fig. 6a, the chronocoulometric signal of *Pf*LDH is similar to that generated from the non-spiked blood sample, which was used as a blank control. In contrast, the chronocoulometric signal from the sample containing *Pf*HRP2 is significantly higher than that of *Pf*LDH, suggesting that our assay is highly specific to *Pf*HRP2. The stability of our sensor was briefly investigated by performing measurements using sensors that were stored for up to 2 weeks at 4 °C. As shown in Fig. 6b, there is no significant difference in the coulometric charges (<2% variation) between the fresh sensors and sensors stored for 1 or 2 weeks.

Table 1 Comparison of enzyme-free electrochemical immunosensors for ultrasensitive analytical measurements

Detection method	Target analyte	Matrix	Limit of detection (LOD)	Detection range	Ref.
Electrochemical–chemical–chemical redox cycling based on graphene and Fe_3O_4/AuNPs	CEA	Tris	0.39 pg mL^{-1}	1 pg mL^{-1}–30 ng mL^{-1}	19
SWV immunoassay based on PdPt nanocages	CEA AFP	PBS and plasma	1.4 pg mL^{-1} 1 pg mL^{-1}	50 ng mL^{-1}–200 ng mL^{-1} 30 ng mL^{-1}–100 ng mL^{-1}	23
Paper based electrochemical immunosensor based on Au–Ag bimetalic nanoparticles	CEA	Plasma	0.3 pg mL^{-1}	1 pg mL^{-1}–50 ng mL^{-1}	40
Electrochemiluminescence based on carbon dots coated silica (SiO_2@C-dots)	CEA PSA AFP	PBS	6 pg mL^{-1} 3 pg mL^{-1} 5 pg mL^{-1}	10 pg ml^{-1}–50 ng mL^{-1}	41
Electrochemical immunosensor based on hybridization chain reaction triggered double strand DNA@Au nanoparticle tag	CEA	Buffer	3.2 fg mL^{-1}	10 fg mL^{-1}–10 ng mL^{-1}	42
Electrochemical—chemical—chemical redox cycling based on methylene blue	*Pf*HRP2	Plasma Whole blood	10 fg mL^{-1} 18 fg mL^{-1}	10 fg ml^{-1}–100 ng mL^{-1}	This work

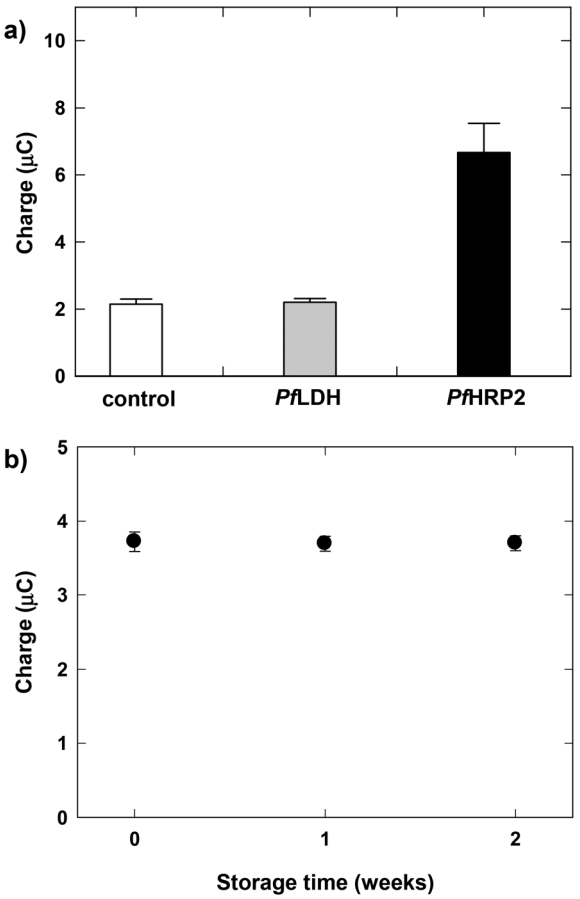

Fig. 6 (a) Chronocoulometric charges of *Pf*HRP2 (1 ng mL^{-1}) and *Pf*LDH (1 ng mL^{-1}) in whole blood and non-spiked blood (blank control). Signals were taken at 100 s from chronocoulograms obtained at 0.05 V. Each bar represents the mean ± SD of three separate measurements using new sensors. (b) Chronocoulometric charges of 1 pg mL^{-1} *Pf*HRP2 in whole blood using fresh sensors and sensors stored for 1 or 2 weeks at 4 °C. Each data point represents the mean ± SD of three separate measurements using new sensors.

Conclusions

We have demonstrated a new enzyme-free electrochemical immunosensor capable of ultrasensitive measurements of protein biomarkers in plasma and whole blood samples. This sensor is based on a unique non-enzymatic ECC redox cycling scheme for signal amplification using MB, $Ru(NH_3)_6^{3+}$ and TCEP. Experiments to study the electrokinetics of this ECC redox cycling scheme revealed its capability for high signal amplification due to a fast endergonic reaction between $Ru(NH_3)_6^{3+}$ and MB_{red} coupled with a fast exergonic reaction between TCEP and MB_{ox}. For proof of principle, this ECC redox cycling scheme was used for electrochemical measurements of *Pf*HRP2 which could be detected at concentrations down to 10 fg mL^{-1} and 18 fg mL^{-1} in plasma and whole blood samples, respectively. Furthermore, this sensor exhibits high specificity, excellent reproducibility, and good stability for up to 2 weeks when stored at 4 °C. In addition to its excellent analytical performance, this sensor does not require complicated sensor modification procedures or detection protocols that are typically associated with redox cycling techniques. These collective features make this immunosensor very promising for several important biomedical applications, including early stage disease diagnosis and non-invasive diagnostic testing.

Conflicts of interest

There are no conflicts to declare.

Acknowledgements

This work was supported by the National Institutes of Health (R01 AI113257).

References

1 J. A. Ludwig and J. N. Weinstein, *Nat. Rev. Cancer*, 2005, **5**, 845.
2 D. A. Giljohann and C. A. Mirkin, *Nature*, 2009, **462**, 461.
3 Z. Sonner, E. Wilder, J. Heikenfeld, G. Kasting, F. Beyette, D. Swaile, F. Sherman, J. Joyce, J. Hagen, N. Kelley-Loughnane and R. Naik, *Biomicrofluidics*, 2015, **9**, 031301–031301.
4 L. Zhou, R. W. Beuerman, C. M. Chan, S. Z. Zhao, X. R. Li, H. Yang, L. Tong, S. Liu, M. E. Stern and D. Tan, *J. Proteome Res.*, 2009, **8**, 4889.
5 Y.-H. Lee and D. T. Wong, *Am. J. Dent.*, 2009, **22**(4), 241.
6 D. G. Georganopoulou, L. Chang, J.-M. Nam, C. S. Thaxton, E. J. Mufson, W. L. Klein and C. A. Mirkin, *Proc. Natl. Acad. Sci. U. S. A.*, 2004, **102**, 2273.
7 C. S. Thaxton, R. Elghanian, A. D. Thomas, S. I. Stoeva, J.-S. Lee, N. D. Smith, A. J. Schaeffer, H. Klocker, W. Horninger, G. Bartsch and C. A. Mirkin, *Proc. Natl. Acad. Sci. U. S. A.*, 2009, **106**, 18437.
8 J. Wang, *Biosens. Bioelectron.*, 2006, **21**, 1887.
9 H. Yang, *Curr. Opin. Chem. Biol.*, 2012, **16**, 422.
10 B. S. Munge, A. L. Coffey, J. M. Doucette, B. K. Somba, R. Malhotra, V. Patel, J. S. Gutkind and J. F. Rusling, *Angew. Chem., Int. Ed.*, 2011, **50**, 7915.
11 G. C. Jensen, X. Yu, J. D. Gong, B. Munge, A. Bhirde, S. N. Kim, F. Papadimitrakopoulos and J. F. Rusling, *J. Nanosci. Nanotechnol.*, 2009, **9**, 249.
12 G. Dutta, S. Kim, S. Park and H. Yang, *Anal. Chem.*, 2014, **86**, 4589.
13 G. Dutta, S. Park, A. Singh, J. Seo, S. Kim and H. Yang, *Anal. Chem.*, 2015, **87**, 3574.
14 A. Walter, J. Wu, G.-U. Flechsigc, D. A. Haaked and J. Wang, *Anal. Chim. Acta*, 2011, **689**, 29.
15 M. R. Akanda, M. A. Aziz, K. Jo, V. Tamilavan, M. H. Hyun, S. Kim and H. Yang, *Anal. Chem.*, 2011, **83**, 3926.

16 A.-M. J. Haque, J. Kim, G. Dutta, S. Kim and H. Yang, *Chem. Commun.*, 2015, **51**, 14493.
17 M. R. Akanda and H. Ju, *Anal. Chem.*, 2016, **88**, 9856.
18 J. Das, I. Ivanov, L. Montermini, J. Rak, E. H. Sargent and S. O. Kelley, *Nat. Chem.*, 2015, **7**, 569.
19 D. Peng, R.-P. Liang, H. Huang and J.-D. Qiu, *J. Electroanal. Chem.*, 2016, **761**, 112.
20 M. R. Akanda, Y.-L. Choe and H. Yang, *Anal. Chem.*, 2012, **84**, 1049.
21 M. R. Akanda, V. Tamilavan, S. Park, K. Jo, M. H. Hyun and H. Yang, *Anal. Chem.*, 2013, **85**, 1631.
22 C. S. Fang, K. H. Oh, A. Oh, K. Lee, S. Park, S. Kim, J. K. Park and H. Yang, *Chem. Commun.*, 2016, **52**, 5884.
23 N. Liu, F. Feng, Z. Liu and Z. Ma, *Microchim. Acta*, 2015, **182**, 1143.
24 R.-D. Li, Q. Wang, B.-C. Yin and B.-C. Ye, *Biosens. Bioelectron.*, 2016, **77**, 995.
25 P. Si, Y. Huang, T. Wang and J. Ma, *RSC Adv.*, 2013, **3**, 3487.
26 W. Wang, Y. Wang, L. Tu, T. Klein, Y. Feng and J.-P. Wang, *IEEE Trans. Magn.*, 2013, **49**, 296.
27 S. Singal, A. K. Srivastava, S. Dhakate, A. M. Biradara and Rajesh, *RSC Adv.*, 2015, **5**, 74994.
28 Y. Guo, Y. Han, Y. Guo and C. Dong, *Biosens. Bioelectron.*, 2013, **45**, 95.
29 M. Tichoniuk, M. Ligaj and M. Filipiak, *Sensors*, 2008, **8**, 2118.
30 X. Lin, Y. Ni and S. Kokot, *Anal. Chim. Acta*, 2015, **867**, 29.
31 Z.-G. Yu and R. Y. Lai, *Anal. Chem.*, 2013, **85**, 3340.
32 H. Ma, Y. Wang, D. Wu, Y. Zhang, J. Gao, X. Ren, B. Du and Q. Wei, *Sci. Rep.*, 2016, **6**, 19797.
33 J. Umbreit, *Am. J. Hematol.*, 2007, **82**, 134.
34 S. Kakhki, M. M. Barsan, E. Shams and C. M. A. Brett, *Anal. Methods*, 2013, **5**, 1199.
35 L. Wu, J. Wang, H. Sun, J. Ren and X. Qu, *Adv. Healthcare Mater.*, 2014, **3**, 588.
36 J. H. Chua, R.-E. Chee, A. Agarwal, S. M. Wong and G.-J. Zhang, *Anal. Chem.*, 2009, **81**, 6266.
37 M. A. Aziz, S. Patra and H. Yang, *Chem. Commun.*, 2008, 4607.
38 D. C. Harris, *Quantitative Chemical Analysis*, Craig Bleyer, New York, 7th edn, 2007, p. 84.
39 J. Wang, *Electroanalysis*, 2001, **13**, 983.
40 G. Sun, Y.-N. Ding, C. Maa, Y. Zhang, S. Ge, J. Yu and X. Song, *Electrochim. Acta*, 2014, **147**, 650.
41 Y. Zhang, W. Liu, S. Ge, M. Yan, S. Wang, J. Yu, N. Li and X. Song, *Biosens. Bioelectron.*, 2013, **41**, 684.
42 Y. Gea, J. Wua, H. Jua and S. Wub, *Talanta*, 2014, **120**, 218.